# Supporting Information for

# Uniform Fluorescent Nanobioprobes for Pathogen Detection

Ling-Hong Xiong,[†] Ran Cui,[†] Zhi-Ling Zhang,[†] Xu Yu,[†] Zhixiong Xie,[§] Yun-Bo Shi,[‡] Dai-Wen Pang[*,†]

[†]Key Laboratory of Analytical Chemistry for Biology and Medicine (Ministry of Education), College of Chemistry and Molecular Science, State Key Laboratory of Virology, and Wuhan Institute of Biotechnology, Wuhan University, Wuhan 430072, People's Republic of China

[§]College of Life Sciences, Wuhan University, Wuhan, 430072, People's Republic of China

[‡]Section on Molecular Morphogenesis, PCRM, NICHD, NIH, Bethesda, Maryland 20892-5431, United States

*Address correspondence to dwpang@whu.edu.cn

Supplementary Text

## Supplementary Note 1

### Characterization of the productivity of the cellular beacons

The colocalization of bright field images and the corresponding the fluorescence images of the cellular beacons was used to determine the productivity of the fluorescing cells. The microscopic analysis of bright field and the corresponding fluorescence images showed that over 99% (essentially 100%) of *S. aureus* cells in bright field had fluorescence (Figure S1).

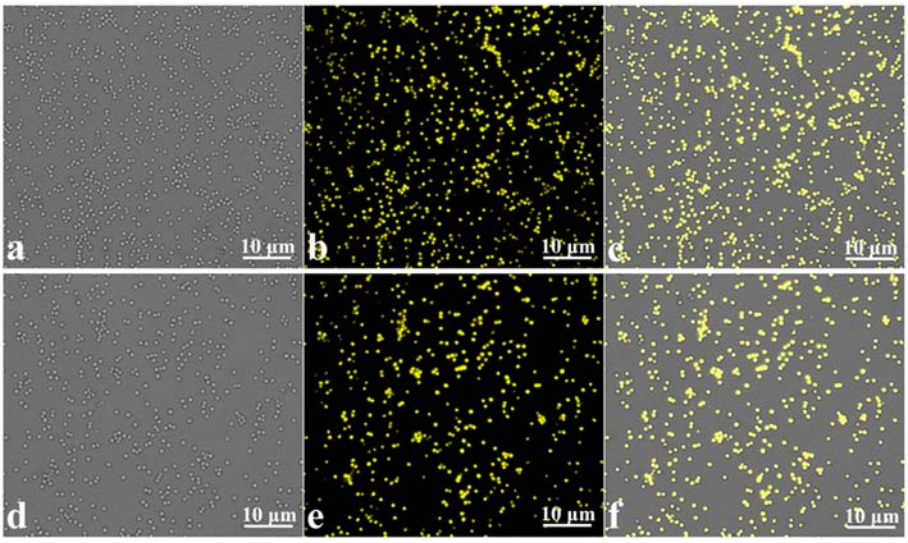


**Figure S1. Productivity of the cellular beacons**. Bright field and fluorescence field images (a and b) of the fluorescing cells after incubation in a 65 °C water bath for 30 min, the merge image (c) of (a) and (b). d-f, as a-c, respectively, except for cells incubated in a 65 °C water bath for 30 min after placing at 4 °C for two months.

## Supplementary Note 2

### Supplementary characterization of $CdS_{0.5}Se_{0.5}$ QDs synthesized *in vivo*.

Fluorescent QDs synthesized *in vivo* were isolated as described in the Methods. The isolated fluorescent QDs were characterized by several additional analyses as described below.

*Photoluminescence characterization for the isolated $CdS_{0.5}Se_{0.5}$ QDs*

The fluorescence spectra of the isolated $CdS_{0.5}Se_{0.5}$ QDs were taken on the Horiba Jobin Yvon Inc Fluorolog-3 spectrophotometer. The yellow emission from the quantum dots was observed, with a Stokes shifted emission maxima at ~520 nm and a second weaker component at ~460 nm from control autofluorescence (Figure S2a). However, the full width at half maximum (fwhm) of the PL emission peak was 143 nm due to the presence of biological molecules such as proteins. The yellow light was bright under the excitation of a UV lamp (Figure S2b), while the control had weak blue autofluorescence from lysates (Figure S2c). Photostability of the isolated $CdS_{0.5}Se_{0.5}$ QDs was characterized with continuous illumination by mercury lamp at a power of 50 W. After 8 h of continuous illumination, the $CdS_{0.5}Se_{0.5}$ QDs retained 100% of their fluorescence (Figure S3a). The results showed that the biosynthesized $CdS_{0.5}Se_{0.5}$ QDs had excellent photostability. Moreover, the $CdS_{0.5}Se_{0.5}$ QDs displayed good photostability when placed at 4 °C for several months (Figure S3b). Even in presence of high concentrations of sodium chloride, the fluorescence intensity of $CdS_{0.5}Se_{0.5}$ QDs was not affected (Figure S3c). Thus, $CdS_{0.5}Se_{0.5}$ QDs showed high fluorescence intensity and good photostability.

*Energy-dispersive X-ray*

Energy-dispersive X-ray (EDX) data (Figure S4) of intracellular QDs and the isolated QDs confirmed that the products consisted of elements Cd, S and Se.

*Analysis of the atomic composition of the nanoprarticles synthesized in vivo.*

The isolated nanoparticles from cells were subjected to element analysis by ICP-AES. The results showed that they had a molar ratio of element Cd to S to Se as 1: 0.5: 0.5 (Table S1).

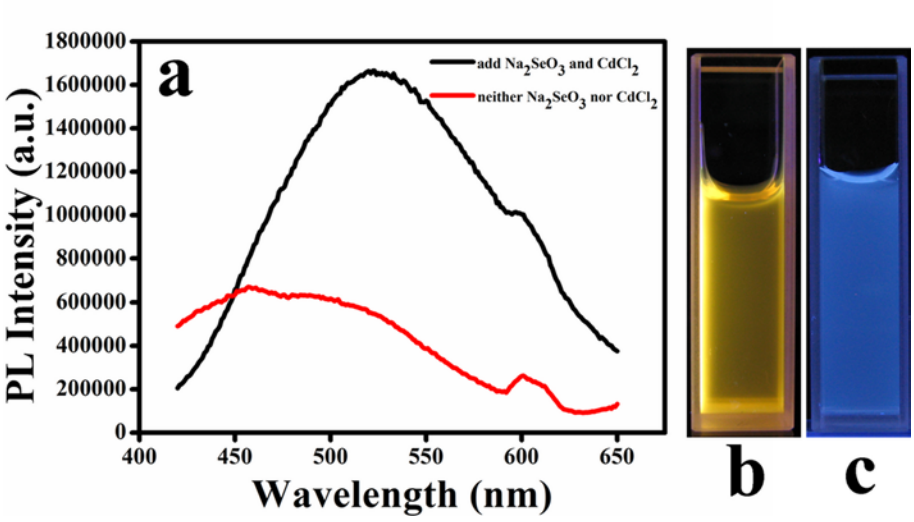


**Figure S2.** (a) Fluorescence spectra of the isolated of $CdS_{0.5}Se_{0.5}$ QDs from the fluorescing *S. aureus* cells (black line) *vs.* the control cells without adding chemicals (red line). (b)/(c) Fluorescence image of the aqueous lysate of *S. aureus* containing $CdS_{0.5}Se_{0.5}$ QDs (b) or the control cell lysate (c) under a UV lamp. The samples were purified with the Amicon Centrifugal Filter Unit (MWCO 10 kDa) to remove free small substances.

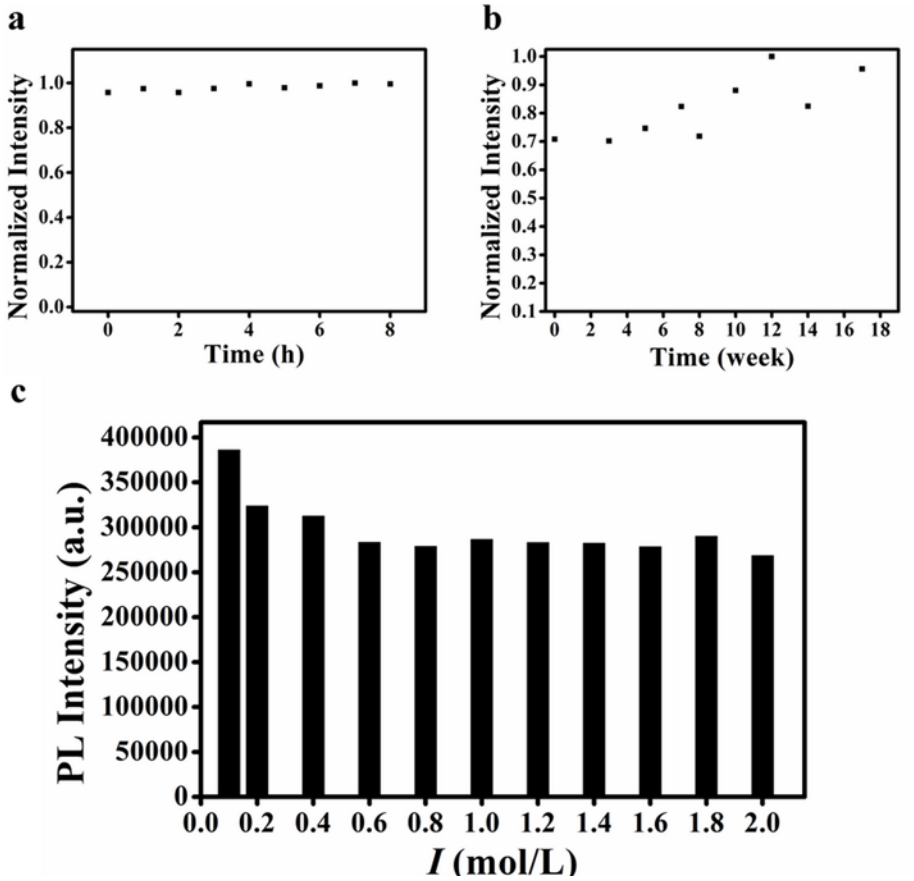


**Figure S3. The characterization of photostability of the isolated $CdS_{0.5}Se_{0.5}$ QDs.** Photostability of the biosynthesized $CdS_{0.5}Se_{0.5}$ QDs with continuous illumination from a mercury lamp (a), after storing at 4 °C for 2 months (b), or in the presence of NaCl solution at the different concentrations (c).

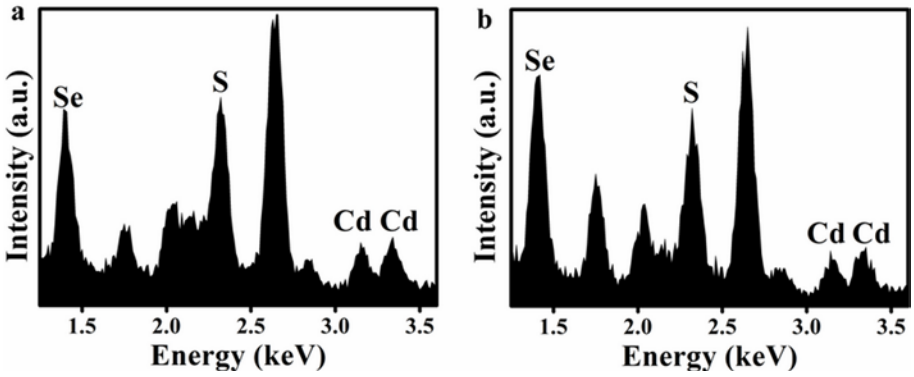

**Figure S4. Characterization of Energy-dispersive X-ray spectroscopy.** (a) *In situ* Energy-dispersive X-ray spectroscopic analysis of intracellular $CdS_{0.5}Se_{0.5}$ QDs. (b) EDX spectrum of the isolated $CdS_{0.5}Se_{0.5}$ QDs.

**Table S1.**

Atomic compositions of isolated nanoprticles.

| Sample | Cd (mg/L) | S (mg/L) | Se (mg/L) |
|---|---|---|---|
| Concentration | 3.1 | 0.5 | 1.2 |
| Relative molar ratio | 1 | 0.5 | 0.5 |

## Supplementary Note 3

**Functional characterization of the activity of the protein A on the cell surface.**

The cellular beacons were harvested by centrifuging at 4000 rpm for 5 min, washed three times with Tris-HCl buffer (pH 8.0, 0.1 M), and then resuspended in the same Tris-HCl buffer. The cellular beacons (OD=1.5, the final volume of 100 μL) incubated at 65 °C water bath for 30 min were mixed with 2 μL of rabbit anti-mouse IgG conjugated with Cy3 (1 mg/mL, Sigma) or just Cy3 (control) for 30 min at 37 °C with shaking at 150 rpm. The cellular beacons were then harvested and washed forth times with Tris-HCl buffer (pH 8.0, 0.1 M) for analysis. The fluorescence microscopy images were shown in Figure S5.

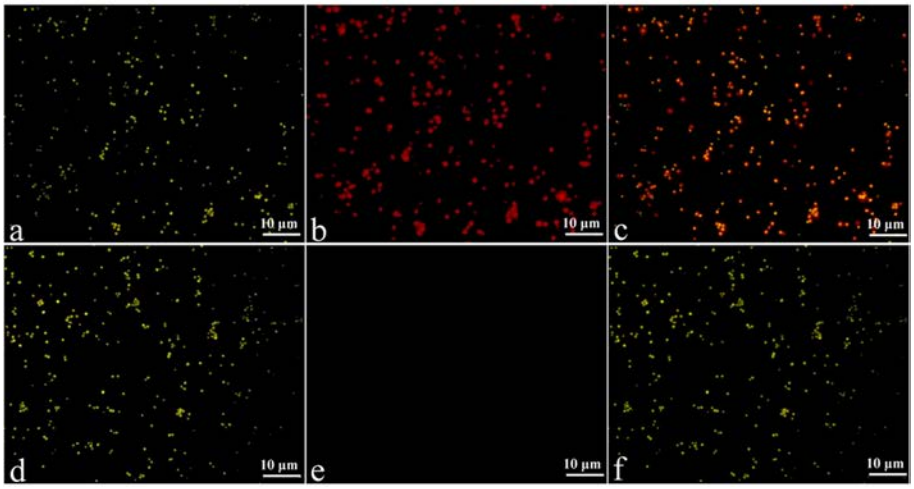


**Figure S5. The characterization of the activity of protein A on the cell surface.** The fluorescence images of the cellular beacons excited by blue light (a and d). (b/e) Immunofluorescence micrograph showing the fluorescence of Cy3 of cells incubated with rabbit anti-mouse IgG conjugated with Cy3 (b) or Cy3 (e) and excited with green light. The merge photos of a and b (c), d and e (f).

## Supplementary Note 4

### Characterization of the mAbs conjugated to the superparamagnetic beads.

Dynamic light scattering (DLS, Zetasizer Nano ZS90, Malvern Instruments) was used to determine the average hydrodynamic diameters of beads and immunomagnetic beads. The hydrated particle sizes of the beads and immunomagnetic beads were found to be about 503.8 nm and 657.3 nm, respectively (Figure S6). The average hydrodynamic diameter increased from 503.8 nm to about 657.3 nm after coupling the Abs to the beads, consistent with Abs conjugated to the beads. Moreover, we used FITC labeled goat anti-mouse IgG to demonstrate that the anti-HA antibody was conjugated to the beads. As

shown in Figure S7b, the green fluorescence of FITC on the anti-HA-beads was obvious compared to the control beads with no green fluorescence due to the binding of anti-HA antibody to the goat anti-mouse IgG-FITC.

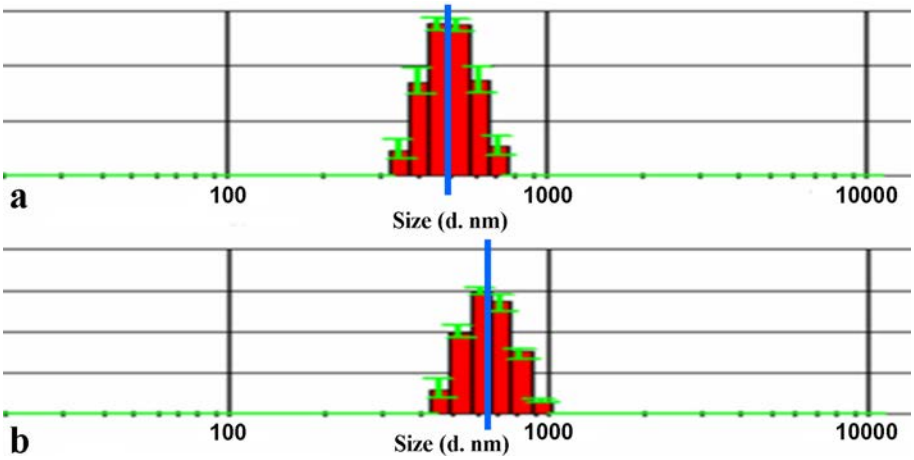


**Figure S6. Characterization of mAbs-conjugated magnetic beads.** (a) The average hydrodynamic diameter of the magnetic beads was measured to be about 503.8 nm. (b) The average hydrodynamic diameter of the anti-HA-magnetic beads was about 657.3 nm.

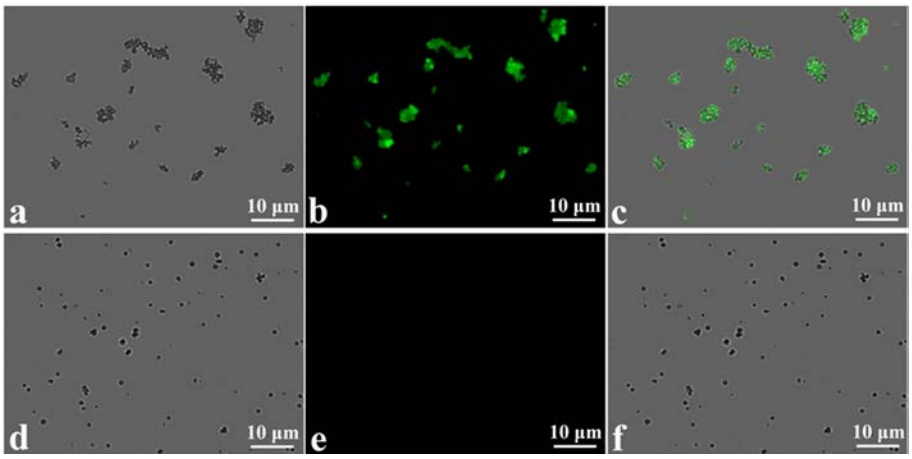

**Figure S7. Characterization of mAbs-conjugated magnetic beads.** Bright field (a, d) and fluorescence field images (b, e) of the magnetic beads (d, e) and the immune complex of immunomagnetic beads (a, b) in the presence of goat anti-mouse IgG-FITC. The merge of a and b (c), d and e (f).

## Supplementary Note 5

**Other negative controls for detecting H9N2 virus.**

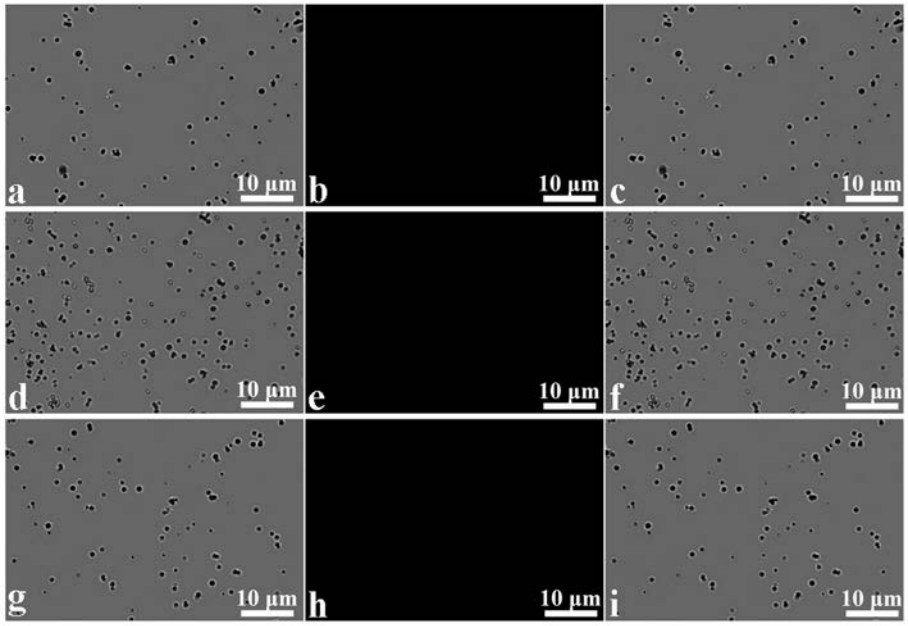


**Figure S8. Other negative controls for detecting H9N2 virus.** The fluorescence images of NDV (b), baculovirus (e) and PRV (h), respectively. Bright field from the corresponding areas of NDV sample (a), baculovirus sample (d) and PRV sample (g), respectively. The merge of a and b (c), d and e (f), g and h (i).

## Supplementary Note 6

**Fluorescent-biotargeting cells as probes for diverse studies.**

*Detection of other viruses*

In order to investigate the possible applications of the fluorescent-biotargeting bifunctional probes to detect other viruses, pseudorabies virus (PRV) and baculovirus were used to desmonstrate the universality of our method. The viruses were quantitated with a standard protein quantification method.[1, 2] The preparation of immunomagnetic beads and mAb-bound *S. aureus* were the same as for H9N2 virus detection except that the monoclonal anti-HA antibodies were replaced by the monoclonal anti-gE antibodies (Jeno Biotech Inc) or anti-gp64 antibodies (eBioscience) (The glycoprotein gE and gp64 are envelope proteins expressed on the surface of the PRV and baculovirus, respectively). Then, the superparamagnetic beads conjugated with monoclonal anti-gE and anti-gp64 antibodies should enable to target recognize the surface protein gE and gp64 of PRV and baculovirus, respectively. As shown in Figure S9, when bead-PRV and bead-baculovirus complexes reacted with fluorescent-biotargeting bacteria, respectively, we obtained similar detection results as with H9N2 AIV detection. Figure S9a-e showed the fluorescence images of detection of PRV with different concentrations ($2.72\times10^3$, $2.72\times10^2$, 27.2, 2.72 and 0 ng/mL, respectively) taken with a cold CCD camera with 1600 ms exposure time. Figure S9f showed the average number of fluorescence dots in twenty random fields, which each concentration repeated three times. Figure S9g-l showed the fluorescence images of detection of baculovirus with different concentrations ($1.38\times10^3$, $1.38\times10^2$, 13.8, 1.38 and 0 ng/mL, respectively). The limits of detection were 2.72 ng/mL and 1.38 ng/mL for PRV and baculovirus, respectively.

*Detection of Salmonella typhimurium (S. typhimurium)and SK-BR-3 cells*

*Salmonella typhimurium* (*S. typhimurium*), *Shigella flexneri* (*S. flexneri*) and *Escherichia coil* (*E. coil*) were provided by Tongji hospital of HuBei province. *S. typhimurium, S. flexneri* and *E. coil* were grown on the MacConkey agar at 37 °C for 24 h. A single colony was picked from agar plate and used to prepare bacteria suspension with physiological saline. The suspension was diluted to the proper concentration, then 10 μL of the diluent was plated onto the Mueller-Hinton agar. After incubation of the plates at 37 °C for 24 h, the number of colony forming units per mL (CFU/mL) was determined by counting the colonies grown on the plates. The bacteria were then heated-inactivated for further use.

SK-BR-3 cells (human breast carcinoma cells) were grown in DMEM (Dulbecco's modified Eagle's medium, Gibco) containing 10% fetal bovine serum (FBS, Gibco), 100 units/mL penicillin G sodium and 100 μg/mL streptomycin sulfate at 37 °C in a 5% $CO_2$ atmosphere. Jurkat T cells (human peripheral blood leukemia T cells) and Ramos cells (human B lymphoblastoid cells ) as control groups were maintained in RPMI 1640 medium with 10% fetal bovine serum, 100 units/mL penicillin G sodium and 100 μg/mL streptomycin sulfate at incubated in humidified environment at 37 °C with 5% $CO_2$ atmosphere. Prior to all experiment, the cells were harvested by centrifuging at 1500 rpm for 3 min and re-dispersed in 1 mL of 1 × PBS (pH=7.2). The cell density was determined using a hemocytometer.

The conjugation procedure of immunomagnetic beads was similar as above except that the monoclonal anti-HA antibodies were replaced by the antibodies to *S. typhimurium* (Abcam) or the monoclonal anti-EpCAM antibodies (Sigma-Aldrich). Likewise, the fluorescing cells were bound with the antibodies to *S. typhimurium* or the

monoclonal anti-EpCAM antibodies instead of the monoclonal anti-HA antibodies. The protocol for *S. typhimurium* and SK-BR-3 cells detection was the same as used the virus detection.

Figure S10 showed the specificity of the bioprobes for *S. typhimurium* detection. We used Tris-HCl (0.1 M, pH=8.0) buffer as the reagent blank to replace *S. typhimurium*, other bacteria such as *S. flexneri* and *E. coil* as the negative control, and $10^7$ CFU/mL *S. typhimurium* as the positive sample. The fluorescence microscopy images (Figure S10b) showed that the fluorescence from the biotargeting cellular beacons was obviously observed in the *S. typhimurium* sample, while no obvious fluorescence from the biotargeting cellular beacons was observed in the controls (Figure S10e, h, k). Thus, the immunomagnetic beads and the mAb-bound fluorescing cells specifically captured and detected *S. typhimurium*. The TEM image (Figure S11a) showed that the immunomagnetic beads bound to *S. typhimurium* cell surface, which further confirmed the bacteria captured by immunomagnetic beads. Furthermore, the immune complex of beads-*S. typhimurium*-biotargeting cellular beacons was shown in Figure S11b, indicating the association between the immunomagnetic beads, *S. typhimurium* and the biotargeting cellular beacons. We also tried to detect *S. typhimurium* at different concentrations and obtained similar results as with the H9N2 AIV detection (Figure S12). With the decreasing of the concentration of target bacteria, the number of the fluorescence dots and the degree of aggregation of immune complex decreased correspondingly.

The above studies clearly demonstrated that target virus and bacteria could be specifically detected in our method. To investigate whether our method could be used for effective detection of the target cells, we next analyzed the SK-BR-3 cells that applied to

detect in our method. The fluorescence microscopic images (Figure S13) showed the fluorescence of the fluorescing cells, which came from the SK-BR-3 cell surface. However, no cells and no fluorescence were found in the controls.

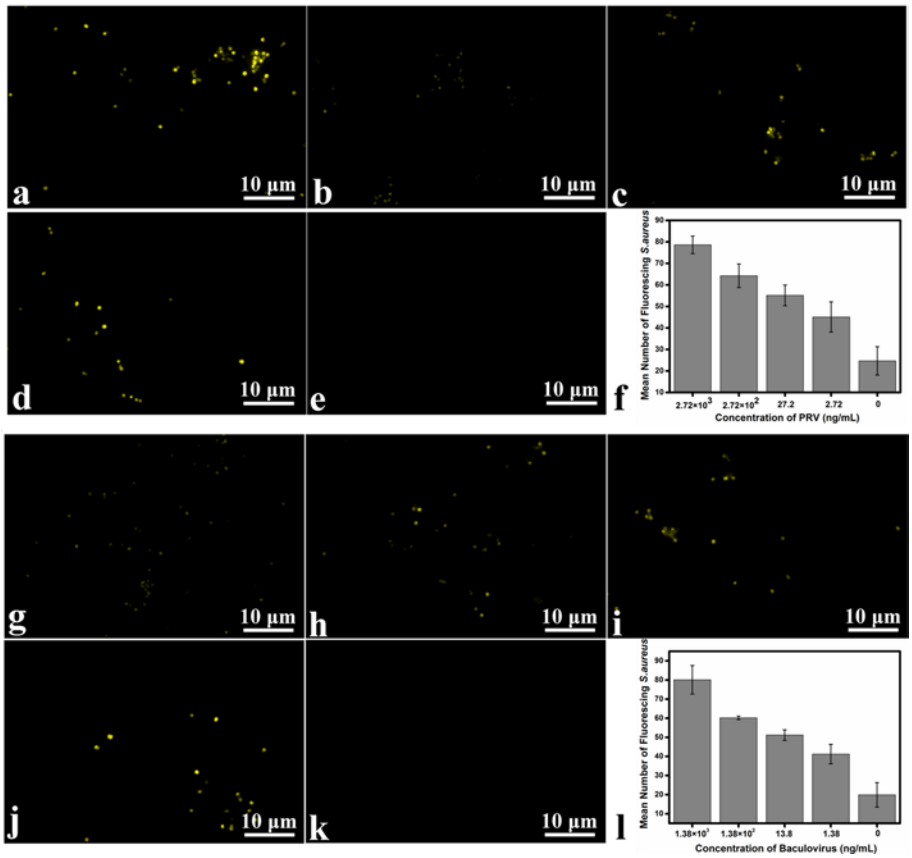


**Figure S9. The detection of PRV and baculovirus.** (a, b, c, d, e) Fluorescence images of detection of PRV at different concentrations ($2.72\times10^3$, $2.72\times10^2$, 27.2, 2.72 and 0 ng/mL, respectively). (f) Histogram from the corresponding concentrations of PRV. (g, h, i, j, k) Fluorescence images of detection of baculovirus at different concentrations ($1.38\times10^3$, $1.38\times10^2$, 13.8, 1.38 and 0 ng/mL, respectively). (l) Histogram from the corresponding concentrations of baculovirus.

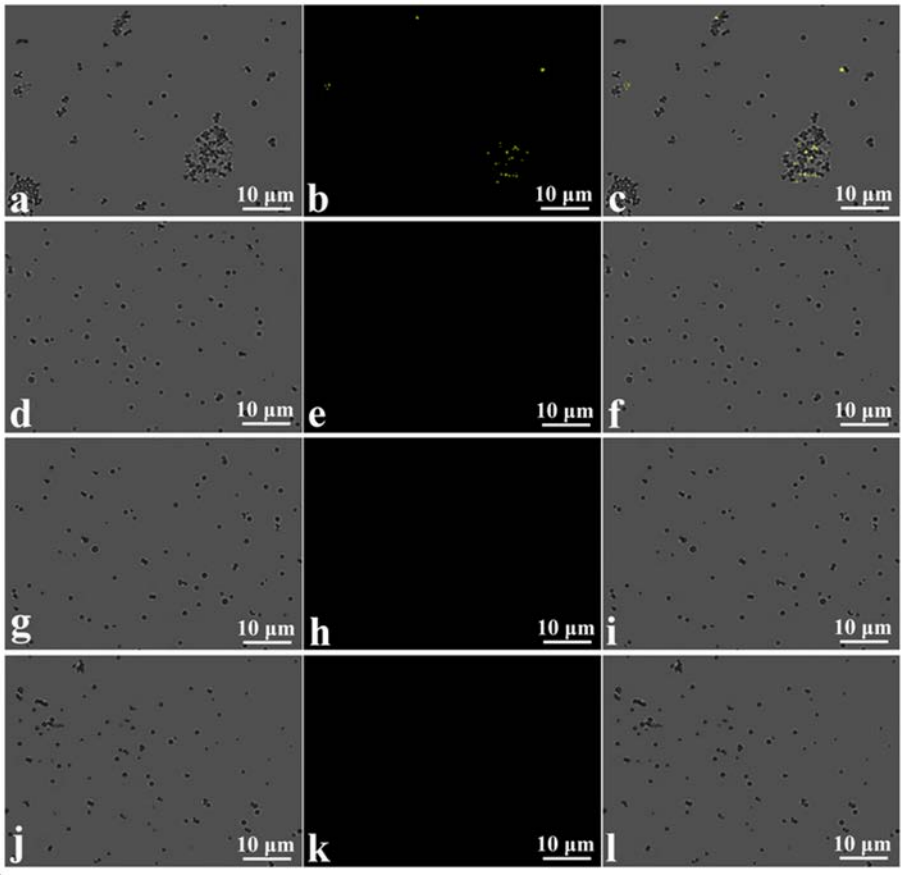


**Figure S10. The detection of *S. typhimurium*.** Fluorescence images of *S. typhimurium* (b), *S. flexneri* (e), *E. coil* (h), and PBS buffer blank (k) captured and identified by immunomagnetic beads and mAb-bound cellular beacons. The bacteria concentrations were $10^7$ CFU/mL. (a, d, g, j) Bright fields from the corresponding fluorescence fields. The merge of a and b (c), d and e (f), g and h (i), j and k (l).

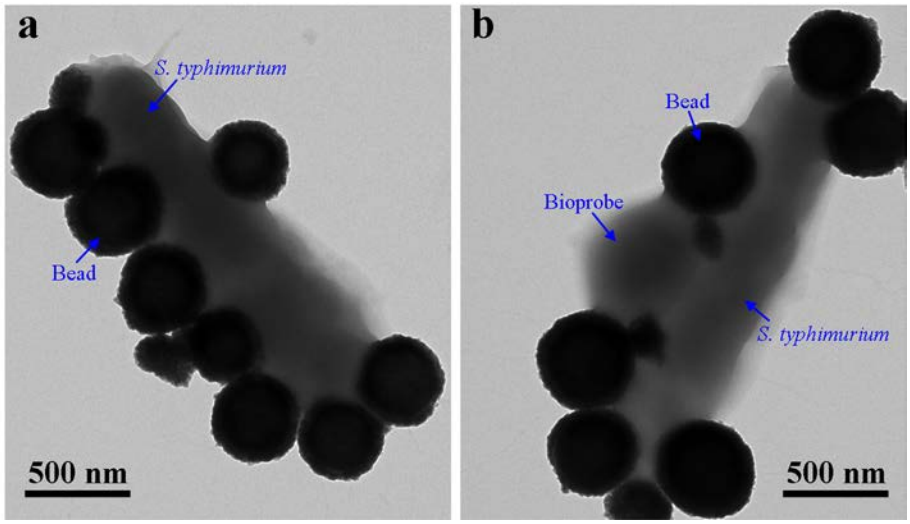


**Figure S11.** (a) TEM image of *S. typhimurium* captured by immunomagnetic beads. (b) TEM image of *S. typhimurium* captured and identified with immunomagnetic beads and mAb-bound cellular beacons (bioprobes).

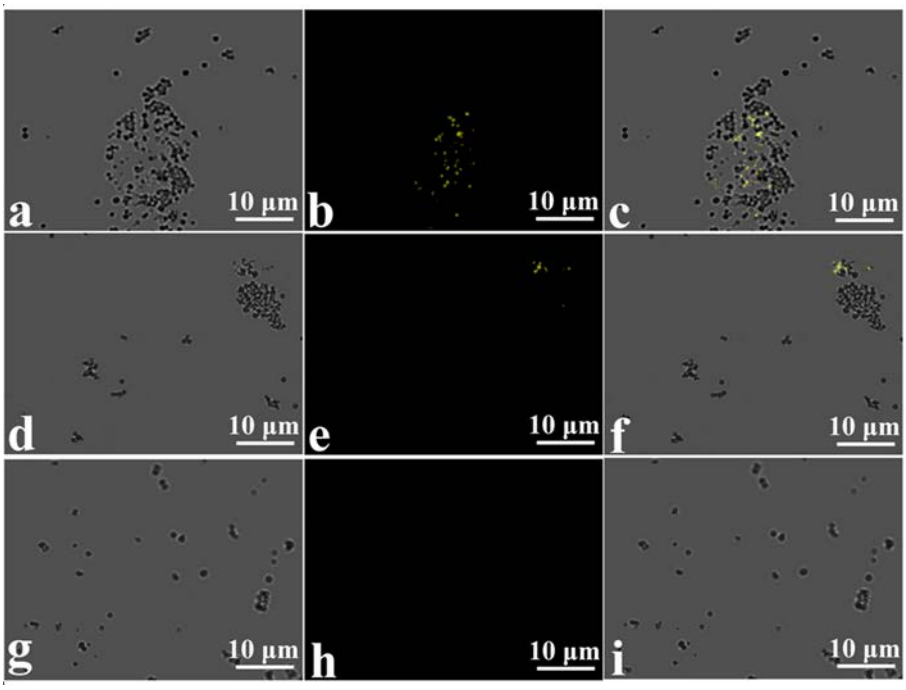

**Figure S12.** (b, e, h) Fluorescence images of detection of *S. typhimurium* at different concentrations ($10^7$, $10^6$ and $10^5$ CFU/mL, respectively). (a, d, e) Bright fields from the corresponding areas of fluorescence fields. The merge of a and b (c), d and e (f), g and h (i).

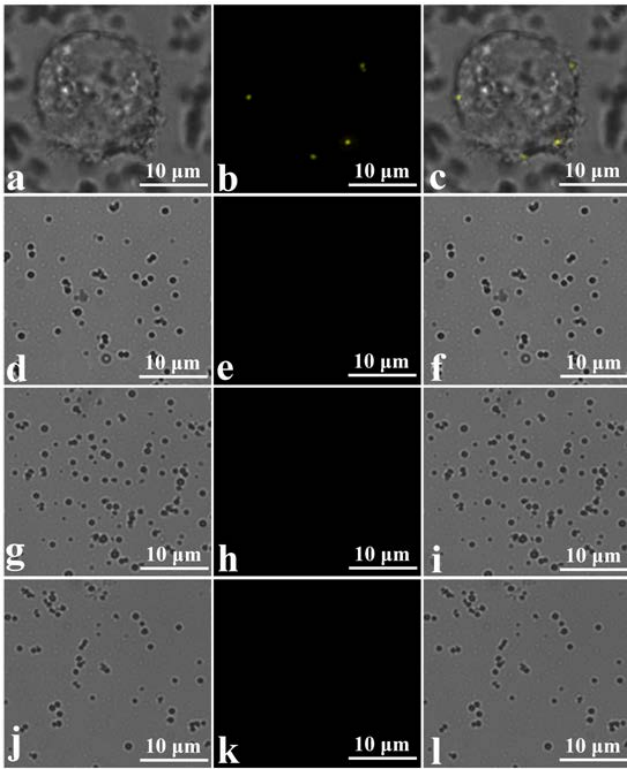


**Figure S13. The detection of SK-BR-3.** Fluorescence images of SK-BR-3 cells ($1.3\times10^5$ per mL) (b), Jurket T cells ($1.3\times10^5$ per mL) (e), Ramos cells ($1.3\times10^5$ per mL) (h), and 1×PBS buffer (pH=7.2) blank (k) captured and identified by immunomagnetic beads and mAb-coated fluorescing cells. (a, d, g, j) Bright fields from the corresponding areas of fluorescence fields. The merge of a and b (c), d and e (f), g and h (i), j and k (l).

## References


1. Chen, L.; Zhang, X.; Zhang, C.; Zhou, G.; Zhang, W.; Xiang, D.; He, Z.; Wang, H. Dual-Color Fluorescence and Homogeneous Immunoassay for the Determination of Human Enterovirus 71. *Anal. Chem.* **2011**, *83*, 7316-7322.

2. Liu, S.-L.; Zhang, Z.-L.; Tian, Z.-Q.; Zhao, H.-S.; Liu, H.; Sun, E.-Z.; Xiao, G.-F.; Zhang, W.; Wang, H.-Z.; Pang, D.-W. Effectively and Efficiently Dissecting the Infection of Influenza Virus by Quantum-Dot-Based Single-Particle Tracking. *ACS Nano* **2012**, *6*, 141-150.